Transconductance Amplifier for Optical Metrology Applications of Light-Emitting Diodes

Timo Dönsberg, Tuomas Poikonen, and Erkki Ikonen

***Abstract*— Light-emitting diodes (LEDs) have many applications in optical metrology. Depending on the measurement scheme, an LED might be driven, for example, using constant current, amplitude or pulsewidth modulated current, or current pulses. We present the design and characterization of a transconductance amplifier (TCA) optimized to drive LEDs in optical metrology applications. The device is capable of delivering peak and root mean square (rms) currents up to 10 and 1 A, respectively, and has a selectable transconductance ranging from 100 μS to 10 S. The typical cutoff frequency for the current output is around 10 MHz for various types of LEDs.**

***Index Terms*— Light-emitting diode (LED), optical metrology, pulsewidth modulation, transconductance amplifier (TCA).**

I. Introduction

LIGHT-EMITTING diodes (LEDs) are an essential part of optical metrology. First, the optical, electrical, and thermal properties of LEDs are an important part of fundamental and applied research. Second, LEDs are used as light sources in a wide variety of metrological applications. Third, there is a recent interest in replacing incandescent lamp-based calibration sources with LED-based solutions [1]–[4].

Current through an LED varies approximately exponentially with applied voltage, and it is also temperature-dependent. Therefore, LEDs are typically driven with current instead of voltage. While constant current is often used, many measurement techniques require the use of current pulses [5]–[7], pulsewidth modulation (PWM) [7]–[10], amplitude modulation (AM) [11], [12], or more complex modulation schemes [13], [14].

In addition to nonlinear current-to-voltage characteristics, LEDs can also have a large junction capacitance, or the measurement setup may be such that large parasitic capacitances and inductances cannot be avoided. This may become problematic, especially if high-frequency current signals are used. Furthermore, one must take into account in the design of the drive electronics that most LEDs can handle only a few volts of reverse voltage.

Arbitrary voltage signals can be easily realized with a modern signal generator. These can be converted to current signals using a transconductance amplifier (TCA). As the name suggests, the output current of the TCA is the input voltage multiplied by some transconductance G_m. A large number of TCA implementations have been reported [15]–[26], but none provides a direct solution to the requirement of combining wide frequency and current ranges with high accuracy and stability. Yet, such designs are urgently needed for advanced applications of LED metrology.

In this article, we present the design and characterization of a TCA optimized to drive LEDs in optical metrology applications. The TCA provides selectable transconductance from 100 μS to 10 S, and peak and root mean square (rms) currents of 10 and 1 A, respectively. The design is done using common components and provides an affordable and robust solution for operating different types of LEDs at frequencies ranging from constant current up to 15 MHz.

A similar device as described in this article has been utilized in the PWM-based technique to obtain the LED spectrum at a known temperature [10], and in LED spectrum measurements at cryogenic temperatures, where the pulsed operation is used to minimize the heating of the LED junction [7].

II. Principle of Operation

The principle of operation of the TCA is illustrated in Fig. 1. Our design utilizes a current-feedback operational amplifier (CFOA) that is buffered with a common drain connected N-channel MOSFET. The noninverting input of the CFOA has high impedance similar to that of a conventional voltage-feedback operational amplifier (VFOA), whereas the inverting input has very low input impedance R_i (tens of ohms to just a few ohms). The open-loop output voltage of a CFOA is the feedback current I_{fb} multiplied with the transimpedance R_{tr}, which is typically in the order of megaohms.

As compared to the conventional operational amplifier, the CFOA has the benefit of having high bandwidth, high slew rate, and low distortion that are fairly independent of the closed-loop gain [27]–[30]. In addition, the low impedance of the inverting input reduces the effects of input capacitance. The CFOA has the drawbacks of having higher offset voltages and lower open-loop gain. The former can be compensated in the design, as discussed in Section III, and the effects of

Manuscript received March 4, 2019; accepted July 11, 2019. Date of publication August 16, 2019; date of current version May 12, 2020. The Associate Editor coordinating the review process was Branislav Djokic. *(Corresponding author: Timo Dönsberg.)*

T. Dönsberg and E. Ikonen are with the Metrology Research Institute, Aalto University, 00076 Aalto, Finland, and also with the MIKES Metrology, VTT Technical Research Centre of Finland Ltd., 02044 Espoo, Finland (e-mail: timo.donsberg@vtt.fi).

T. Poikonen is with the MIKES Metrology, VTT Technical Research Center of Finland Ltd., 02044 Espoo, Finland.

Color versions of one or more of the figures in this article are available online at http://ieeexplore.ieee.org.

Digital Object Identifier 10.1109/TIM.2019.2935596

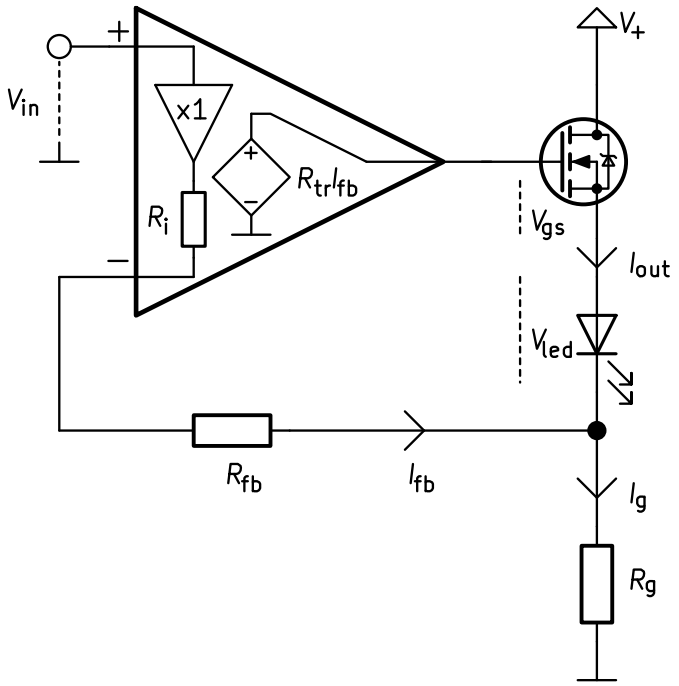

Fig. 1. Basic principle of the TCA.

the latter can be accurately characterized, as demonstrated in Section IV. CFOAs are also optimized for a limited range of feedback resistor values and are sensitive to stray capacitances across the feedback resistor. However, this is not an issue in our design since the feedback circuitry is fixed regardless of the selected transconductance.

As seen in Fig. 1, the output current I_{out} flows through the LED and the shunt resistor R_g, whereas R_{fb} provides the feedback to the inverting input of the CFOA. In an ideal case, the transimpedance R_{tr} of the CFOA is infinite, and the circuitry balances the output current so that the voltage over the shunt resistor R_g is equal to the input voltage. For example, the transconductance is solely determined by the value of R_g and the ideal output current becomes

$$I_{\text{ideal}} = G_m V_{\text{in}} = \frac{V_{\text{in}}}{R_g}. \tag{1}$$

In practice, however, R_{tr} is finite, which causes an error in the output current I_{out}. The error can be approximated by assuming the voltages V_{gs} and V_{led} to be constant. This leads to

$$I_{\text{out}} = \frac{(R_{\text{tr}} - R_g)V_{\text{in}} - (R_i + R_{\text{fb}} + R_g)(V_{\text{led}} + V_{\text{gs}})}{R_g(R_i + R_{\text{fb}} + R_{\text{tr}})}. \tag{2}$$

The situation is actually more complex, since both V_{gs} and V_{led} are current-dependent. Nonetheless, this simple approach serves as an order of magnitude estimation for the error of the output current. Subtracting (1) from (2) yields

$$\begin{aligned}\Delta I_{\text{out}} &= I_{\text{out}} - I_{\text{ideal}} \\ &= -\frac{(R_i + R_{\text{fb}} + R_g)(V_{\text{in}} + V_{\text{led}} + V_{\text{gs}})}{R_g(R_i + R_{\text{fb}} + R_{\text{tr}})}.\end{aligned} \tag{3}$$

Since $R_i \ll R_{\text{fb}} \ll R_{\text{tr}}$, this can be approximated as

$$\Delta I_{\text{out}} \approx -\frac{1}{R_{tr}}\left(1 + \frac{R_{\text{fb}}}{R_g}\right)(V_{\text{in}} + V_{\text{led}} + V_{\text{gs}}). \tag{4}$$

Note that the V_{in}-dependent term of ΔI_{out} can be seen as error in the transconductance value set by R_g, and the other terms as output load-dependent error current. Clearly, both terms become insignificant if R_{tr} is sufficiently large and R_g is not exceedingly small. The effects of limited open-loop gain and other practical limitations are further discussed in Section IV.

III. Practical Design

Simplified schematic of the TCA is shown in Fig. 2. AD810 [31] is used as the CFOA, as it combines high transimpedance (typical value around 3.5 MΩ) with 80 MHz bandwidth and low noise. It also features an offset null option and disable function, both utilized in the design. Although significantly faster CFOAs are available, they tend to have smaller transimpedance. Moreover, as higher bandwidth is not necessary for this application, the excess bandwidth only compromises robustness.

The input of the amplifier is terminated with a 50-Ω low inductance planar thick film power resistor R1. The resistor R6 in the output is mandatory to provide pull-down, as the MOSFET follower Q2 can only increase the output voltage. The value 1 kΩ of R6 was found to be sufficiently small for typical output configurations without having a significant load to the CFOA output. If a high capacitance load is unavoidable, an additional pull-down resistor or synchronized active pull-down circuitry may be used [7].

Having a single MOSFET output instead of a push-pull configuration also has the benefit that the maximum negative output current of the TCA is automatically limited to about 15 mA. This enables the use of low capacitance signal diodes in the TCA output as polarity protection. Such protection is needed in case a negative voltage is accidentally applied to the TCA input or transient spikes occur. Having four 1N4148 diodes in series (D2–D5) limits the minimum output voltage to about −3 V and has a capacitance below 1 pF over a wide frequency range [32].

Signal relays are used to select the transconductance of the amplifier, by effectively changing the value of R_g in 2. For clarity, only one of the six relays and resistors—K1 and R8, respectively—are drawn in Fig. 2. MHP20-series high-frequency and high-power thin-film resistors [33] with resistances ranging from 100 mΩ to 10 kΩ were used as gain selection resistors. The relays are controlled with a microcontroller (MC) in such a way, that when the gain is changed, the disable pin of the CFOA is grounded with the Q1 transistor. In addition to the MC-controlled reset, a delayed reset pull-up circuit consisting of D1, C3, and C4 was added. The former is to avoid unstable operation during gain change and the latter during startup.

The offset nulling option of the CFOA is adjusted in such a way that when the input is unconnected, the output current of the TCA is just above zero. This guarantees that the output is prebiased close to the MOSFET threshold voltage,

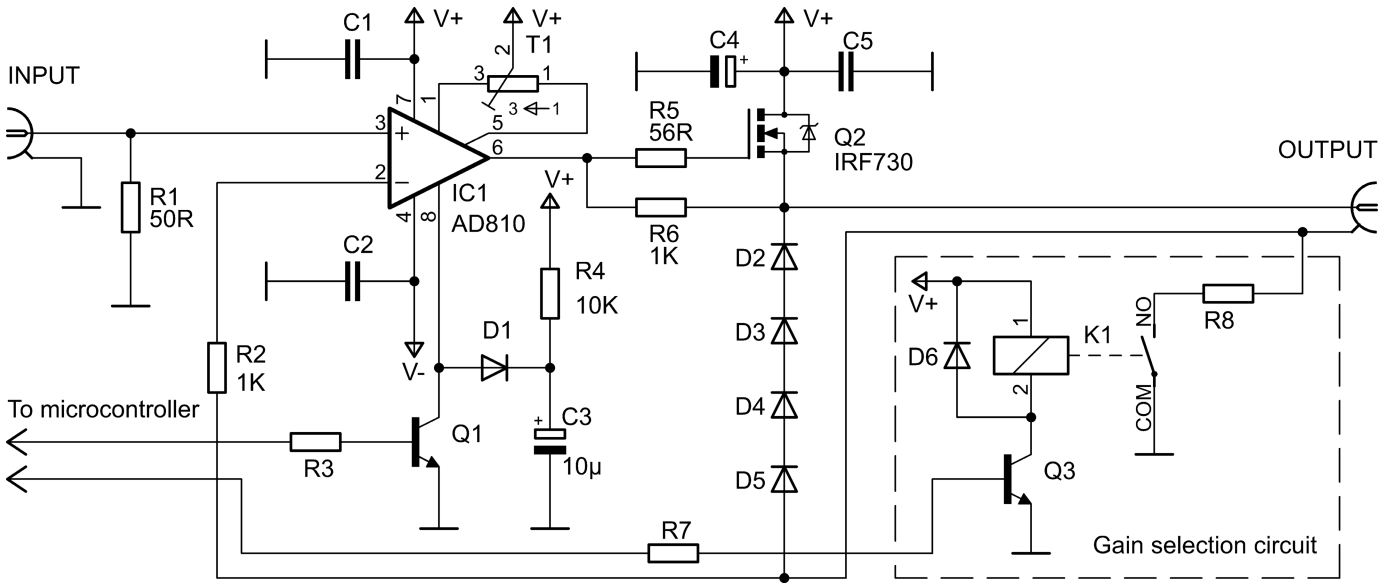

Fig. 2. Simplified schematic of the TCA. Only one gain selection circuit is drawn; the actual device has six similar circuits connected in parallel, out of which one is enabled at a time.

TABLE I
MEASURED TRANSCONDUCTANCE VALUES OF THE TCA. THE UNCERTAINTIES ARE GIVEN AT 95% CONFIDENCE LEVEL

Nominal transconductance	Measured transconductance
100 μS	(99.741 ± 0.011) μS
1 mS	(999.40 ± 0.03) μS
10 mS	(9.9896 ± 0.0007) mS
100 mS	(99.935 ± 0.010) mS
1 S	(975.26 ± 0.31) mS
10 S	(8.494 ± 0.026) S

minimizing the change of V_{gs} in 3. The CFOA controls the gate of the MOSFET Q2 via resistor R5. This prevents parasitic oscillations and ringing of the MOSFET [34].

IV. PERFORMANCE

A. Transconductance and Load-Dependent Error Current

The transconductances of the TCA were calibrated by applying a voltage to the input with a Keithley 263 calibrator and measuring the output current with a Hewlett Packard 3458A multimeter. Since the output resistance of the calibrator affects the voltage seen at the TCA input, the input voltage was also measured with Agilent 34410A multimeter. The calibration results are shown in Table I.

For transconductances of 100 mS and below, most of the deviation from the nominal value is due to the tolerance of gain selection resistors, whereas the uncertainty of the transconductance calibration is dominated by the statistical component of the measurements. For the two highest transconductances, most of the deviation and calibration uncertainty of the transconductance is due to contact resistance of the signal relays. Simple calculation from the deviation of the nominally 10-s transconductance gives an estimation of 18 mΩ for the contact resistance. Based on the fluctuation of the transconductance observed when switched back and forth 20 times, we estimated the standard deviation of the contact resistance to be around 180 $\mu\Omega$. A straightforward improvement would be to use a different type of relays for the highest transconductances or to connect multiple relays in parallel.

As seen from (3), the TCA output has a small load and transconductance-dependent error current. In order to quantify this, the transconductances were also calibrated with a resistor connected in the output of the TCA in series with the multimeter. The resistor values were chosen in such a way that the voltage over the resistor is 1 V. This is effectively the same as changing the value of V_{led} in 3 by 1 V.

Table II shows the measured effect of output load and values calculated using 3. The measured values are a factor of 2–3 smaller than the calculated ones. This is understandable, as the calculations were meant to serve as the order of magnitude estimations. For example, the R_{tr} of a CFOA is inversely dependent on output load resistance [31], and the R_{tr} value specified by the manufacturer assumes the load resistance of the CFOA output to be a factor 2.5 smaller than in our design. Nonetheless, the calculated and measured values are very consistent, and the theoretical model provides a useful tool for understanding the sources of error.

B. Noise

Fig. 3 shows the output current noise of the TCA at different transconductances, measured when the input is disconnected. The noise currents were measured with Hewlett Packard 3458A multimeter that was connected directly to the TCA output. The multimeter was set to ac current measurement mode at 100-μA range, which uses an internal 730-Ω shunt resistor to determine the current. In order to limit the noise

TABLE II
CALCULATED AND MEASURED EFFECT OF OUTPUT LOAD VOLTAGE. THE UNCERTAINTIES ARE GIVEN AT 95% CONFIDENCE LEVEL

Nominal transconductance	Calculated effect of output load	Measured effect of output load
100 μS	-315 nS	(-167 $\pm$ 10) nS
1 mS	-583 nS	(-284 $\pm$ 8) nS
10 mS	-3.26 μS	(-1.8 $\pm$ 0.2) μS
100 mS	-30.0 μS	(-10.6 $\pm$ 1.0) μS
1 S	-297 μS	(-170 $\pm$ 3) μS
10 S	-2.97 mS	(-1.2 $\pm$ 0.4) mS

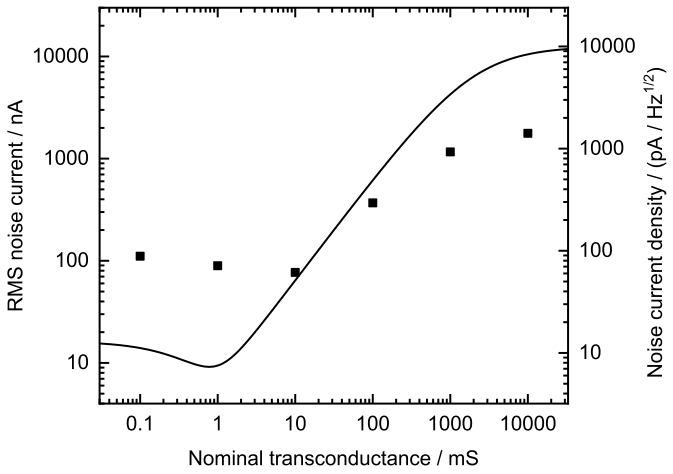

Fig. 3. Measured (squares) and modeled (line) rms noise current of the TCA output. The right axis shows the values converted into noise current density.

signal to a frequency range suitable for the multimeter, a 220-pF capacitor was added to the TCA output. The capacitor—in parallel with the multimeter shunt resistor—acts as a single-pole 1-MHz low-pass filter. The intrinsic noise of the multimeter was quadratically subtracted from the measured values.

The output noise current was also calculated by using a noise model of the measurement scheme. The model takes into account the voltage and current noises of the CFOA and the Johnson–Nyquist noise of the resistors. The measurements indicate a higher noise floor density than the modeled values—an average of around 70 pA/$\sqrt{\text{Hz}}$ for the three smallest transconductances. At higher transconductances, the output noise is more dependent on R_{tr} and the voltage noise of the CFOA. At the highest transconductances, the noise model overestimates the noise level, most likely because the values specified by the manufacturer are given for a smaller output impedance. Moreover, the simple model does not take into account the frequency dependence of these parameters.

C. Bandwidth

The bandwidth of the TCA is limited either by the bandwidth CFOA or the frequency dependence of the shunt resistances. The former was measured with the test setup, shown in Fig. 4, by measuring the voltage over the gain setting resistors inside the device. Since the bandwidth is dependent on the output load, three different loads were tested: short circuit (only a 20-cm wire loop), high-power LED (Kingbrite L-53SRD-E), and low-power LED (Edixeon EDSX-KLC8-E5). The low-power LED was only used with the three smallest transconductance settings. The current output bandwidths were measured with an input signal

$$V_{\text{in}}(t) = \left(0.55 + \frac{\sin(2\pi f t)}{2}\right)\ V \tag{5}$$

except the 10-S transconductance, for which a signal with ten times smaller offset and amplitude was used. The results are shown in Fig. 5.

TABLE III
SMALLEST VALUES OF C_{comp} FOR WHICH PEAKING AT THE OUTPUT CURRENT FREQUENCY RESPONSE DOES NOT OCCUR

	C_{comp} value / nF		
Nominal transconductance	Short circuit	High power LED	Low power LED
100 μS	1.5	1.2	1.8
1 mS	1.2	1.2	1.7
10 mS	1.2	1.9	2.2
100 mS	2	1.8	-
1 S	1.1	1.1	-
10 S	0	0	-

The frequency response of the TCA has shown peaking at frequencies near the 3-dB bandwidth limit. Typically, such features are compensated, for example, by tweaking the feedback or output circuitry, or by adding a capacitor to an internal node of the CFOA [28], [31]. For our purpose, this option was considered somewhat impractical, as the transconductance, output load, and wiring affect the peaking conditions. Instead, the compensation can be done by adding a capacitor (C_{comp} in Fig. 4) in parallel with the TCA input, which forms a low-pass filter with the signal generator output impedance and TCA input impedance. This approach of reference signal filtering has previously been used to compensate for more complex nonlinearities of current generators [35]. Optimal values of C_{comp} for different output loads, *i.e.*, smallest values for which peaking does not occur, are given in Table III. Fig. 5 also shows the bandwidths in the cases when compensation is used.

It should be noted that the use of C_{comp} is not necessary if the highest frequency component of the input voltage is well below the cutoff frequency, or the overshoot is taken into account in the signal generator. The latter is straightforward, for example, if a single modulation frequency is used as it can be achieved simply by adjusting the modulation amplitude.

For the 100-μS transconductance, the parasitic capacitance of shunt resistor begins to affect the frequency response at a smaller frequency than the limit set by the CFOA, reducing the 3-dB bandwidth to 4 MHz [33]. The parasitic inductances of the shunt resistors, on the other hand, limit the usable frequency range of 1 and 10 S transconductances

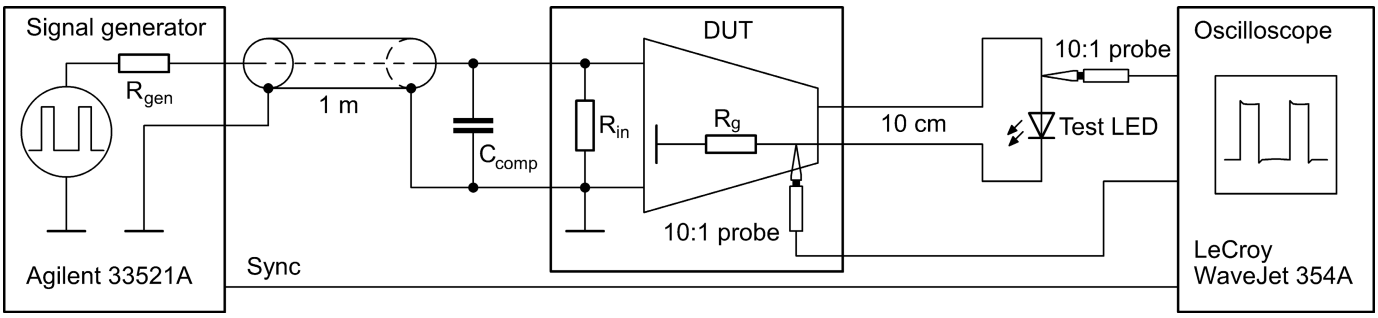

Fig. 4. Schematic of the test measurement setup used to measure the bandwidth and pulsing properties of the TCA.

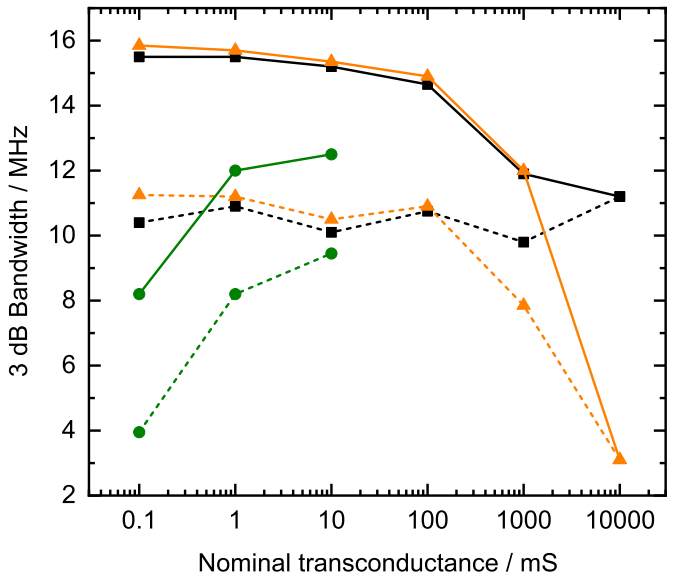

Fig. 5. 3-dB bandwidth of the TCA measured with short circuited output (black squares) and with high-power LED (orange triangles) and small power LED (green circles) as output load. Values with solid lines were measured without C_{comp}, and for values with dashed lines, capacitances listed in Table III were used as C_{comp}.

TABLE IV

TYPICAL BANDWIDTHS OF THE TCA AT DIFFERENT TRANSCONDUCTANCES. THE VALUES ARE TAKEN AS THE AVERAGE OF SHORT CIRCUIT AND HIGH-POWER LED BANDWIDTHS. UNLESS NOTED OTHERWISE, THE BANDWIDTHS ARE LIMITED BY THE CFOA

Nominal trans-conductance	3 dB Bandwidth / MHz	
	With C_{comp}	Without C_{comp}
100 μS	4[a]	4[a]
1 mS	11	16
10 mS	10	15
100 mS	11	15
1 S	9	10[b]
10 S	1[b]	1[b]

[a] Limited by the shunt resistor capacitance.
[b] Limited by the shunt resistor inductance.

to 10 and 1 MHz, respectively, [33]. The usable frequency ranges of the TCA are summarized in Table IV.

D. Pulsed Operation

One of the main applications of the TCA is to provide sharp current pulses for LEDs. The sharpness of a current pulse is limited by the rise and fall time of the TCA, which is closely related to the bandwidth of the system. For an ideal single-pole low-pass filter, the relationship between 10% and 90% rise time (or corresponding fall time) and the cutoff frequency f_c is

$$t_r = \frac{\ln 9}{2\pi f_c} \approx \frac{0.35}{f_c}. \quad (6)$$

The current output rise and fall times of the TCA, measured also with the setup of Fig. 4, were remarkably close to what one would expect based on 6. Typical deviation from

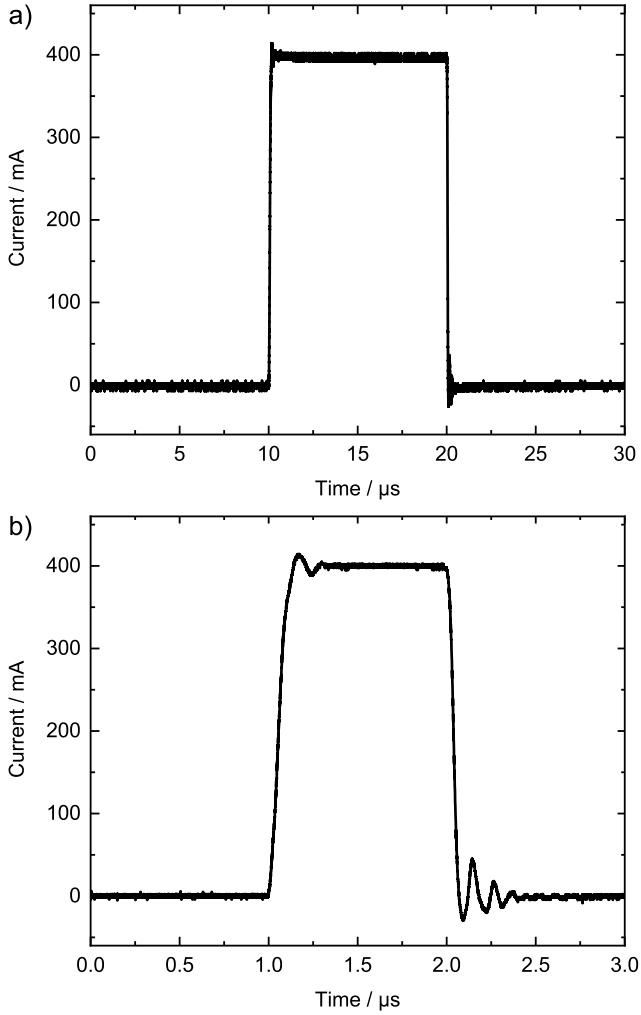

Fig. 6. Current pulses of 400 mA having the widths of 10 μS (a) and 1 μS (b). Pulses were produced with the transconductance setting of 100 mS and with the high-power LED as output load. $C_{\text{comp}} = 1.8$ nF was used in the TCA input. Part of the observed overshoot may arise from the overshoot of the signal generator, which is specified to be 2%.

the expected value was in the order of few nanoseconds. Therefore, in the transconductance range of 1 mS–1 S, *i.e.*, in ranges where shunt resistors do not limit the bandwidth, pulse widths down to 1 μS remain reasonably sharp, assuming the wiring can be kept short and parasitic capacitances small. Examples of 1- and 10-μS current pulses, measured using the setup of Fig. 4, are shown in Fig. 6.

V. Conclusion

In this article, a TCA based on MOSFET buffered CFOA was presented. Intuitively, practical limitations of the CFOA, such as the limited transimpedance and the error caused by feedback current, would appear to limit its use in metrological applications, where high accuracy is mandatory. In our article, we have theoretically shown and demonstrated in practice that these error terms are sufficiently small that they can be accurately characterized.

The fairly simple design of the TCA is constructed using common and affordable components. It provides selectable transconductance from 100 μS to 10 S, and peak and rms currents of 10 and 1 A, respectively. Regardless of the type of LED used in the output or the transconductance, 1-MHz bandwidth was achieved for the TCA. For the transconductances of 1-mS–1-S, typical bandwidth is around 10 MHz without peaking in the frequency response of the output current. If peaking is acceptable, bandwidths up to 15 MHz are achievable.

There are examples of TCAs with higher bandwidth [25], [26], higher output current [15]–[18], or higher precision [15]. However, our device provides a unique combination of these properties optimized for various applications of LEDs in optical metrology.

References

[1] J.-M. Hirvonen, T. Poikonen, A. Vaskuri, P. Kärhä, and E. Ikonen, "Spectrally adjustable quasi-monochromatic radiance source based on LEDs and its application for measuring spectral responsivity of a luminance meter," *Meas. Sci. Technol.*, vol. 24, no. 11, Sep. 2013, Art. no. 115201.

[2] T. Pulli, T. Dönsberg, T. Poikonen, F. Manoocheri, P. Kärhä, and E. Ikonen, "Advantages of white LED lamps and new detector technology in photometry," *Light, Sci. Appl.*, vol. 4, no. 9, Sep. 2015, Art. no. e332.

[3] A. Kokka *et al.*, "Development of white LED illuminants for colorimetry and recommendation of white LED reference spectrum for photometry," *Metrologia*, vol. 55, no. 4, pp. 526–534, Jun. 2018.

[4] M.-M. Sildoja *et al.*, "LED-based UV source for monitoring spectroradiometer properties," *Metrologia*, vol. 55, no. 3, pp. S97–S103, Apr. 2018.

[5] Y. Xi and E. Schubert, "Junction–temperature measurement in GaN ultraviolet light-emitting diodes using diode forward voltage method," *Appl. Phys. Lett.*, vol. 85, no. 12, pp. 2163–2165, Sep. 2004.

[6] Y. Zong and Y. Ohno, "New practical method for measurement of high-power LEDs," in *Proc. CIE Expert Symp. Adv. Photometry Colorimetry*, Jul. 2008, pp. 102–106.

[7] E. Martikainen, A. Vaskuri, T. Dönsberg, and E. Ikonen, "Cryostatsetup for measuring spectral and electrical properties of light-emitting diodes from 78 K to 296 K," submitted for publication.

[8] P. Manninen and P. Orreveteläinen, "On spectral and thermal behaviors of AlGaInP light-emitting diodes under pulse-width modulation," *Appl. Phys. Lett.*, vol. 91, no. 18, Nov. 2007, Art. no. 181121.

[9] V. I. Smirnov, V. A. Sergeev, and A. A. Gavrikov, "Apparatus for measurement of thermal impedance of high-power light-emitting diodes and LED assemblies," *IEEE Trans. Electron Devices*, vol. 63, no. 6, pp. 2431–2435, Jun. 2016.

[10] A. Vaskuri *et al.*, "Relationships between junction temperature, electroluminescence spectrum and ageing of light-emitting diodes," *Metrologia*, vol. 55, no. 2, pp. S86–S95, Mar. 2018.

[11] A. Kimachi, H. Ikuta, Y. Fujiwara, M. Masumoto, and H. Matsuyama, "Spectral matching imager using amplitude-modulation-coded multispectral light-emitting diode illumination," *Proc. SPIE*, vol. 43, no. 4, pp. 975–986, Apr. 2004.

[12] A. C. Terracciano *et al.*, "Hazardous gas detection sensor using broadband light-emitting diode-based absorption spectroscopy for space applications," *New Space*, vol. 6, no. 1, pp. 28–36, Mar. 2018.

[13] A. Dubois, L. Vabre, A.-C. Boccara, and E. Beaurepaire, "High-resolution full-field optical coherence tomography with a Linnik microscope," *Appl. Opt.*, vol. 41, no. 4, pp. 805–812, 2002.

[14] W. Zhao *et al.*, "Detection of micro/nano-particle concentration using modulated light-emitting diode white light source," *Sens. Actuators A, Phys.*, vol. 285, pp. 89–97, Jan. 2019.

[15] N. Wang, Z. Li, Z. Zhang, Q. He, B. Han, and Y. Lu, "A 10-A high-precision DC current source with stability better than 0.1 ppm/h," *IEEE Trans. Instrum. Meas.*, vol. 64, no. 6, pp. 1324–1330, Jun. 2015.

[16] O. B. Laug, "A 100 A, 100 kHz transconductance amplifier," *IEEE Trans. Instrum. Meas.*, vol. 45, no. 2, pp. 440–444, Apr. 1996.

[17] P. Weßkamp, P. Haußmann, and J. Melbert, "600-a test system for aging analysis of automotive li-ion cells with high resolution and wide bandwidth," *IEEE Trans. Instrum. Meas.*, vol. 65, no. 7, pp. 1651–1660, Jul. 2016.

[18] Y. Zhang, N. Wang, Z. Li, B. Han, and X. Li, "A 10-A wideband transconductance amplifier," in *Proc. Conf. Precis. Electromagn. Meas. (CPEM)*, Jul. 2016, pp. 1–2.

[19] H.-J. Chiu and S.-J. Cheng, "LED backlight driving system for large-scale LCD panels," *IEEE Trans. Ind. Electron.*, vol. 54, no. 5, pp. 2751–2760, Oct. 2007.

[20] M. Wan, W. Liao, K. Dai, and X. Zou, "A nonlinearity-compensated all-MOS voltage-to-current converter," *IEEE Trans. Circuits Syst., II, Exp. Briefs*, vol. 63, no. 2, pp. 156–160, Feb. 2016.

[21] W. Surakampontorn, V. Riewruja, K. Kumwachara, C. Surawatpunya, and K. Anuntahirunrat, "Temperature-insensitive voltage-to-current converter and its applications," *IEEE Trans. Instrum. Meas.*, vol. 48, no. 6, pp. 1270–1277, Dec. 1999.

[22] W. Tangsrirat, "Gm-realization of controlled-gain current follower transconductance amplifier," *Sci. World J.*, vol. 2013, Oct. 2013, Art. no. 201565.

[23] A. Mahnam, H. Yazdanian, and M. M. Samani, "Comprehensive study of howland circuit with non-ideal components to design high performance current pumps," *Measurement*, vol. 82, pp. 94–104, Mar. 2016.

[24] V. G. Sirtoli, V. C. Vincence, and P. Bertemes-Filho, "Mirrored enhanced Howland current source with feedback control," *Rev. Sci. Instrum.*, vol. 90, no. 2, Feb. 2019, Art. no. 024702.

[25] M. Mathew, K. Hayatleh, and B. L. Hart, "A high-transconductance voltage-to-current converter design," *Circuits, Syst. Signal Process.*, vol. 29, no. 6, pp. 1123–1140, Dec. 2010.

[26] V. R. A. Cleber, A. Oliveira, and C. S. F. Raimundo, "A new low power and all-MOS voltage-to-current converter for current mode ADCs with high linearity, high bandwidth and rail-to-rail input range," in *Proc. 3rd Int. Symp. Instrum. Syst., Circuits Transducers (INSCIT)*, Aug. 2018, pp. 1–6.

[27] B. J. Maundy, I. G. Finvers, and P. Aronhime, "Alternative realizations of CMOS current feedback amplifiers for low voltage applications," *Analog Integr. Circuits Signal Process.*, vol. 32, no. 2, pp. 157–168, Aug. 2002.

[28] R. Mita, G. Palumbo, and S. Pennisi, "Low-voltage high-drive CMOS current feedback op-amp," *IEEE Trans. Circuits Syst., II, Exp. Briefs*, vol. 52, no. 6, pp. 317–321, Jun. 2005.

[29] A. Tammam, K. Hayatleh, S. Barker, M. Ben-Esmael, and N. Terzopoulos, "Improved designs for current feedback op-amps," *Int. J. Electron. Lett.*, vol. 4, no. 2, pp. 215–227, 2016.

[30] A. Tammam, K. Hayatleh, S. Barker, and N. Terzopoulos, "Theoretical study of the circuit architecture of the basic CFOA and testing techniques," *Int. J. Electron.*, vol. 103, no. 9, pp. 1475–1497, 2016.

[31] Analog Devices. (1992). *AD810—Low Power Video op Amp With Disable*. [Online]. Available: https://www.analog.com/media/en/technical-documentation/data-sheets/AD810.pdf

[32] M. A. R. B. L. Fernandes and E. J. P. Santos, "Measurement of p-n-junction diode behavior under large signal and high frequency," in *Proc. 29th Symp. Microelectron. Technol. Devices (SBMicro)*, Sep. 2014, pp. 1–4.

[33] *MHP20 Datasheet—20W To-220 HIGH Power Resistors*. London, U.K.: TT Electronics, 2011.

[34] B. T. Azizoğlu and H. Karaca, "Investigating a MOSFET driver (buffer) circuit transition ringings using an analytical model," *IEEE Trans. Power Electron.*, vol. 30, no. 9, pp. 5058–5066, Sep. 2015.

[35] L. Cristaldi, M. Faifer, C. Laurano, R. Ottoboni, S. Toscani, and M. Zanoni, "A low-cost generator for testing and calibrating current transformers," *IEEE Trans. Instrum. Meas.*, vol. 68, no. 8, pp. 2792–2799, Aug. 2018.

Timo Dönsberg was born in Rauma, Finland, in 1985. He received the B.Sc., M.Sc., and D.Sc. (Tech.) degrees from Aalto University, Espoo, Finland, in 2009, 2012, and 2017, respectively.

He is currently a Senior Scientist with the Environmental Metrology Group, Centre for Metrology MIKES that is part of VTT Technical Research Centre of Finland Ltd., Espoo, and a Visiting Researcher with the Metrology Research Institute, Aalto University. His current research interests include active hyperspectral spectroscopy, electronics and system design, silicon photodiode-based primary standards of optical power, and the LED photometry and fundamental properties of semiconductor optoelectronics at room temperature and at cryogenic temperatures.

Tuomas Poikonen received the Ph.D. degree from Aalto University, Espoo, Finland, in 2012, with a thesis on characterization of light emitting diodes and photometer quality factors.

In his daily work, he develops electrical, photometric, and radiometric measurement methods for LEDs and OLEDs, and for solar cells. He was a Work Package Leader for project EMRP MESaIL, in which he focused on electrical power measurements and modulation properties of ac-operated LED products, and spectral and angular correction methods for measurements with integrating spheres. He is currently a Senior Scientist with the Electrical Metrology Group, Centre for Metrology MIKES that is part of VTT Technical Research Centre of Finland Ltd., Espoo. VTT MIKES is the National Metrology Institute (NMI) of Finland and provides metrological calibrations, research, and development services for the industry. He is currently coordinating the project EMPIR Future Photometry Based on SSL products (PhotoLED) that develops new LED calibration sources and measurements methods for photometry, supporting the global change of lighting products to LEDs. He has ten years of experience in maintaining the photometric quantities of Finland.

Dr. Poikonen is a member of several other CIE TCs. He is currently the Chair of the Technical Committee CIE TC2-90 LED Reference spectrum for photometer calibration.

Erkki Ikonen received the M.Sc. and D.Sc. (Tech.) degrees in engineering from the Helsinki University of Technology, Espoo, Finland, in 1982 and 1988, respectively.

Until 1988, he was with the Department of Technical Physics, Helsinki University of Technology, where he was engaged in basic research of experimental physics. From 1988 to 1989, he was with the Electrical Engineering Laboratory, VTT Technical Research Center of Finland Ltd., Espoo. Since 1989, he has been with the Metrology Research Institute, Aalto University, Espoo, where he has been a Professor of measurement science and technology since 1995. Since 2005, he has been a Joint Professor with MIKES Metrology, VTT Technical Research Center of Finland Ltd. He has authored more than 180 peer-reviewed publications. His current research interests include the development of laser-based measurements and improved methods for radiometric and photometric measurements.

Dr. Ikonen has acted as the Chair of the European Metrology Research Program from the beginning of 2016 and the Vice-President Technical of the International Commission on Illumination (CIE), from the summer of 2015. From 2005 to 2014, he was the Chairman of the Scientific Committee of NEWRAD Conference, New Developments and Applications in Optical Radiometry.